Radiation Pressure Backaction on a Hexagonal Boron Nitride Nanomechanical Resonator

Irene Sánchez Arribas, Takashi Taniguchi, Kenji Watanabe, and Eva M. Weig*
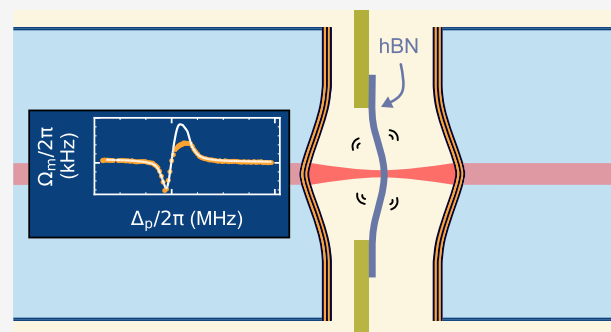
ACCESS | Metrics & More | Article Recommendations | Supporting Information

ABSTRACT: Hexagonal boron nitride (hBN) is a van der Waals material with excellent mechanical properties hosting quantum emitters and optically active spin defects, with several of them being sensitive to strain. Establishing optomechanical control of hBN will enable hybrid quantum devices that combine the spin degree of freedom with the cavity optomechanical toolbox. In this Letter, we report the first observation of radiation pressure backaction at telecom wavelengths with a hBN drum-head mechanical resonator. The thermomechanical motion of the resonator is coupled to the optical mode of a high finesse fiber-based Fabry−Pérot microcavity in a membrane-in-the-middle configuration. We are able to resolve the optical spring effect and optomechanical damping with a single photon coupling strength of $g_0/2\pi = 1200$ Hz. Our results pave the way for tailoring the mechanical properties of hBN resonators with light.

KEYWORDS: optomechanics, microcavity, hexagonal boron nitride, nanomechanical resonators, 2D materials

Part of the current research efforts in the field of cavity optomechanics[1] focuses on implementing nanomechanical resonators based on low dimensional materials, such as carbon nanotubes,[2−5] nanowires,[6] or van der Waals materials.[7−10] Their low mass makes them very sensitive and responsive to external stimuli, and their large zero-point fluctuations x_{zpf} provide large optomechanical single-photon couplings g_0, necessary to manipulate the mechanical or optical states in the quantum regime.[11−13]

Hexagonal boron nitride (hBN) has recently caught the attention of the optomechanics community. Its large in-plane Young's modulus of 392 GPa[14] and breaking strain of 12.5%[15] together with the recent development of patterning methods[16,17] have opened the door to the engineering of mechanical resonators with high quality factors and tunable frequencies. This layered crystal is transparent in the visible and infrared part of the optical spectrum due to its wide bandgap of 6 eV[18] and therefore is less prone to photothermal heating than other van der Waals materials like graphene. So far, photothermal forces, rather than radiation pressure, were responsible for the optomechanical backaction observed in other two-dimensional resonators in the optical regime, limiting their performance.[19−21]

Moreover, perhaps one of the most appealing characteristics of hexagonal boron nitride is its large variety of single-photon emitters. They span from the UV to the low infrared,[22,23] are tunable via strain or electric fields,[24−27] and are capable of operating at room temperature and up to 800 K.[28] Experimental works over the past three years[29−31] have demon-

strated optically detected magnetic resonance in negatively charged boron vacancy defects (V_B^-), together with coherent control of the spins.[32,33] A recent study on these vacancies has shown control at room temperature of a protected qubit basis, with a coherence time as high as 0.8 μs.[34] These spin defects are also sensitive to strain,[35,36] making hBN a promising material to develop the field of spin-mechanics and spin-optomechanics.[37,38] Indeed, these hybrid systems could enable the communication between photons and qubits within hBN, a new step toward quantum networks and quantum communication and an alternative system to the leading platform of nitrogen vacancy centers in diamond.

Given these remarkable properties, it is natural to study how to use radiation pressure to control and modify the mechanical properties of hBN resonators. However, optomechanical dynamical backaction has not yet been observed with resonators made of this van der Waals material. Indeed, the attempts to perform cavity optomechanical experiments with hBN resonators are scarce: the first available platforms for hBN cavity optomechanics experiments are mechanically exfoliated hBN resonators coupled to the near-field of a microdisk
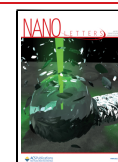
cavity.[39,40] Shandilya et al.[39] were able to measure the thermal motion of a hBN beam through its optomechanical interaction with a silicon microdisk cavity in the telecom regime for the first time, with a sensitivity of 0.16 pm/$\sqrt{\text{Hz}}$. Nevertheless, no optomechanical backaction was observed.

In this paper, we report the first demonstration of radiation pressure backaction with a hexagonal boron nitride circular drum-head resonator at room temperature. We achieve this by inserting the nanomechanical resonator in a high finesse fiber-based Fabry−Pérot microcavity[41−44] in a membrane-in-the-middle configuration,[1,43,45−48] featuring an optical mode waist 8 times smaller than the drum diameter. The corresponding small mode volume, intrinsic to fiber cavities, is critical to avoid clipping of the cavity mode by the edges of the drum, maintaining the high finesse of the cavity. It allows reducing the resonator's diameter down to some tens of micrometers, which is crucial as large area few-layer flakes are difficult to obtain through mechanical exfoliation.

Figure 1 shows the sample used in this work. It consists of a circular resonator made of a mechanically exfoliated hexagonal
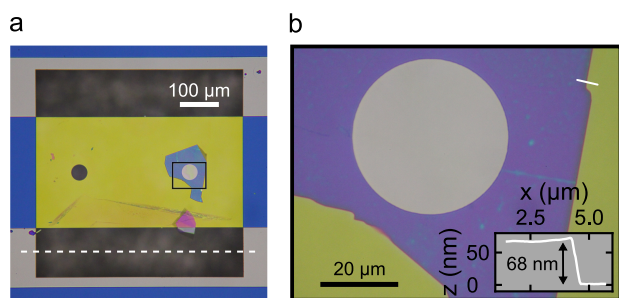

Figure 1. hBN circular membrane. (a) Bright-field microscopy image of the suspended flake (blue) atop a $40\,\mu$m diameter hole patterned on a stripe processed from a commercial SiN membrane (yellow). The frame of the SiN membrane is cleaved along the white dashed line next to the stripe to allow inserting the mechanical resonator inside the optical cavity. (b) Zoom into the black rectangle from (a). The inset shows the AFM height profile along the white line in the top-right corner of the micrograph.

boron nitride flake. The flake rests on a $40\,\mu$m diameter circular hole patterned on a broad $500 \times 281\,\mu\text{m}^2$ stripe. The hole and the stripe are etched from a commercially available low stress 200 nm thick SiN membrane (Norcada) via standard photolithography and reactive ion etching. The crystal is transferred onto the hole through the all-dry viscoelastic method[49] and cleaned with O_2 plasma (300 W, 100 sccm, 90 Pa, 3 min). Its thickness is measured with an atomic force microscope in tapping mode, revealing a thickness of 68 nm (Figure 1b, inset). Finally, the $200\,\mu$m thick silicon frame of the SiN membrane is cleaved along the white dashed line in Figure 1a to allow inserting the sample into the fiber-based Fabry−Pérot microcavity.

We identify the mechanical resonances by systematic characterization in a standard Michelson interferometer. Following the work from Jaeger et al.,[50] we use the experimentally determined effective mass to characterize the degree of mechanical hybridization of the hBN resonator with the mechanical modes of the SiN stripe supporting the flake (Supporting Information). We observe a series of mechanical modes between 1500 kHz and 1700 kHz that are localized in the circular hBN resonator and possess effective masses more than 1 order of magnitude below that of pure SiN modes,

which we identify as hybridized modes with a strong hBN character. Subsequently, the sample is placed in a high finesse Fabry−Pérot microcavity, operated at λ = 1550 nm. The cavity, illustrated in Figure 2a, consists of two fiber mirrors concavely
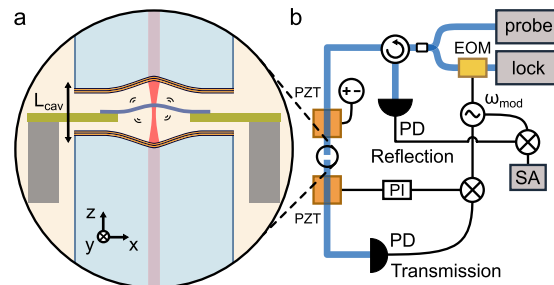
Figure 2. Representation of the experimental setup. (a) The Fabry−Pérot cavity is formed by two fiber mirrors (light blue rods) separated by a length of L_{cav} = 41.8 μm. The suspended hBN (dark blue) on the SiN membrane (SiN in green, Si frame in gray) is inserted between the mirrors by a positioner stack allowing tilt corrections and position scans along the x, y, and z directions. (b) The cavity length is fixed by applying a DC voltage to the top piezo (PZT). The lock laser is phase-modulated at ω_{mod} with an electro-optic modulator (EOM), and its transmission signal is demodulated at ω_{mod} and fed to a PI controller. The latter sends the feedback signal to the bottom piezo, stabilizing the cavity length. The reflection photodetector (PD) signal is sent to a spectrum analyzer (SA) to characterize the mechanical spectra. An additional tunable probe laser is used to measure optomechanical dynamical backaction effects.

shaped by CO_2-laser ablation with a radius of curvature of 190.8 μm for the input fiber (single mode) and 135.6 μm for the output fiber (multimode), respectively, separated by a length of L_{cav} = 41.8 μm. The calculated beam waist is w_0 = 5.1 μm. The fiber ends are ion beam sputtered with a distributed Bragg reflector (LaserOptik GmbH) to obtain a mirror transmission of 10 ppm around λ = 1550 nm. Each of the fiber mirrors is glued to a shear piezo that allows tuning of the cavity length by $\pm$0.7 μm. By scanning the cavity length, we extract the cavity line width $\kappa/2\pi$ = 18.5 MHz and the polarization mode splitting $\Delta\nu_{\text{pol}}$ = 133.5 MHz. The free-spectral range and empty cavity finesse are $\omega_{\text{FSR}}/2\pi$ = 3.584 THz and $\mathcal{F}$ = 194 000, respectively. More details on the cavity characterization methods can be found elsewhere.[41] The sample is placed in a 5-axis positioning system (SmarAct) that allows aligning the sample to the cavity mode axis (z-axis in Figure 2a) and scanning it along the x, y, and z directions. The system is operated at room temperature, in vacuum at a pressure below 10^{-6} mbar, and inside an acoustic isolation box to damp spurious mechanical vibrations. Figure 2b depicts a simplified version of the setup. To perform dynamical backaction experiments, we lock the cavity length to a reference laser (NKT Koheras Basik E15, λ = 1550 nm) referred to in the following as lock laser. The lock laser is phase-modulated at $\omega_{\text{mod}}/2\pi$ = 30 MHz with an electro-optic modulator (EOM). The light transmitted through the cavity, recorded by a fast photodetector (PD), is demodulated at the same frequency and sent to a PI controller that sends the feedback signal to a piezoelectric converter (PZT) to perform the lock. We use the Y-quadrature of the demodulated signal as error signal for the lock. The reflected light from the lock laser is equally demodulated and fed to a spectrum analyzer that records the mechanical spectra. We use an additional probe
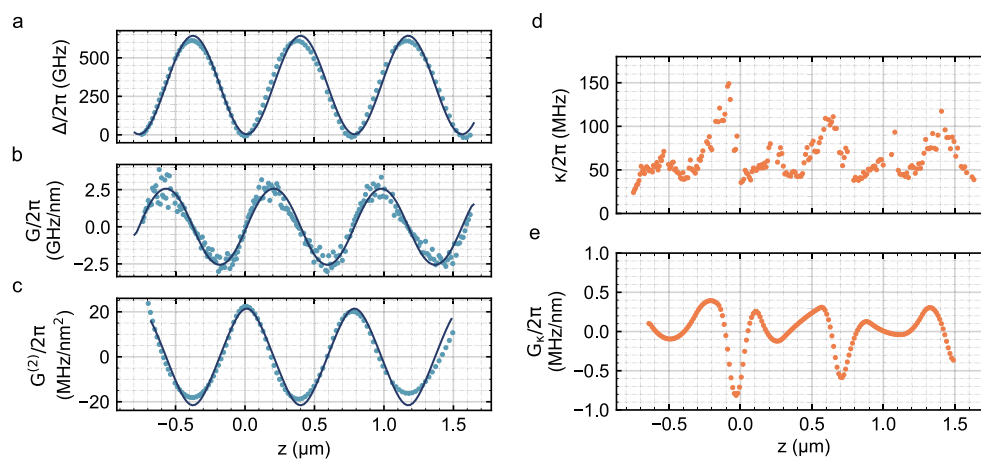
Figure 3. Static optomechanical couplings. (a) Cavity detuning (dots) vs sample position z along the cavity mode axis. The coordinate $z = 0$ corresponds to the sample sitting in an optical field node. (b) Dispersive and (c) quadratic dispersive coupling. The solid lines in (a), (b), and (c) are the result of transfer matrix calculations. (d) Cavity line width modulation and (e) corresponding dissipative coupling.

laser (New Focus TLB-6700) to sweep the wavelength across the cavity resonance and exert an optomechanical force. Both lasers are operated at orthogonal cavity polarizations to avoid interference effects.

The dispersive optomechanical coupling $G = \partial\omega_{cav}/\partial z$ [48] is obtained by measuring the dependence of the detuning of the cavity resonance frequency $\Delta(z)$ as a function of the sample position z along the cavity mode axis. To that end, the system is operated in an open-loop configuration, and both piezos are scanned symmetrically. We use only the lock laser and record the cavity transmission and reflection. We observe a sinusoidal pattern of the detuning (blue dots, Figure 3a) that reaches a maximum of $\Delta/2\pi = 600$ GHz when the sample is placed at the cavity antinodes. We verify that the cavity detuning originated solely from the hBN drum and has no contribution from the surrounding SiN by performing the same measurement on the second, empty 40 μm diameter hole (Supporting Information) shown in Figure 1a. G is directly extracted from the measurement by performing a numerical derivative (blue dots, Figure 3b). We observe a maximum of $|G/2\pi| = 2.5$ GHz/nm. As expected for a membrane-in-the-middle system, the quadratic dispersive coupling $G^{(2)} = \partial^2\omega_{cav}/\partial z^2$ reaches a maximum at the cavity nodes and antinodes,[47,51] of value $|G^{(2)}/2\pi| = 20$ MHz/nm^2 for our system (blue dots, Figure 3c). The quadratic coupling is extracted by smoothing the data from Figure 3b with a spline and computing its numerical derivative. The measurements are well reproduced by transfer matrix calculations[52] (solid lines in Figure 3), with input parameters of a flake thickness of 58 nm and flake refractive index of $n_{hBN} = 1.85$. The reduced thickness originates from an additional O$_2$ cleaning step that etched the flake, which was observed as a change of color under an optical microscope.

Any absorption or scattering from the flake will manifest as a modulation of the cavity line width κ, displayed in Figure 3d. The line width is calculated from the cavity transmission on resonance (see ref 41 for more details) and reaches a minimum value of $\kappa/2\pi \simeq 40$ MHz when the sample is placed at the cavity nodes. hBN has a negligible absorption coefficient at telecom wavelengths,[53,54] and therefore the large cavity line widths we observe cannot be attributed to optical absorption. Performing the same measurements shown in Figure 3d on the SiN membrane results in modulations of the same magnitude (Supporting Information) that cannot be explained consider-

ing the absorption coefficient of SiN. This suggests that the losses in our system are dominated by scattering to higher order optical modes of the cavity originated by a sample misalignment with respect to the cavity mode axis[47,51] and not by remaining impurities from the transfer process. The hypothesis is also consistent with the dips observed at the antinodes and the small scale variations ($z < \lambda$) of the cavity line width.[47] The line width modulation translates into the dissipative coupling $G_{\kappa} = \frac{\partial\kappa}{\partial z}$ (Figure 3e) that we extract by smoothing the data in Figure 3d and performing a numerical derivative. We highlight that dissipative coupling is more than 3 orders of magnitude smaller than the dispersive coupling and is therefore negligible in our system.

To perform dynamical backaction experiments, we place the hBN drum $\Delta z = 13$ nm away from the cavity node. From the cavity transmission, we obtain a loaded cavity line width of $\kappa/2\pi = 39.8(2)$ MHz, yielding a loaded cavity finesse of $\mathcal{F} = 90\,000$. This sample position corresponds to a value of $G/2\pi = 330$ MHz/nm and $G_{\kappa}/2\pi = 0.19$ MHz/nm, extracted from the measurements in Figure 3. We lock the cavity length with a lock power of $P_l = 34.5\,\mu$W and at a frequency ω_{cav} detuned from the lock laser frequency ω_l by $\Delta_l/2\pi = (\omega_l - \omega_{cav})/2\pi = -50$ MHz. We choose this value as a compromise between having a good signal in reflection and minimizing the backaction from the lock. To transform the measured power spectral densities S_V in volts into displacement power spectra densities S_x, we use as reference the thermomechanical spectra of a well characterized SiN mode at 164.0 kHz of known effective mass $m_{eff} = 2.3\,\mu$g when probed at the center of the drum-head, following the calibration procedure described in ref 55. This mode is suitable for calibration because it does not show optomechanical coupling. The conversion factor between displacement and voltage is 3 pm/mV. Figure 4 shows the spectrum of the SiN mode used for calibration, together with the spectrum of the hBN mode used to perform backaction experiments. The solid lines are fits using the displacement power spectral density formula

$$S_x(\omega) = \frac{4\Gamma_0 k_B T}{m_{eff}((\Omega_0^2 - \omega^2)^2 + \Gamma_0^2\omega^2)} \quad (1)$$

where T is the bath temperature, k_B is the Boltzmann constant, and the only fit parameters are the mechanical resonance
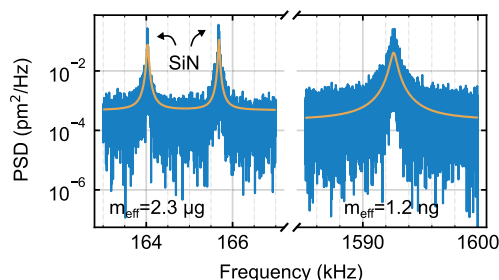
Figure 4. Displacement power spectral density (PSD) measured with the locked cavity. Two SiN modes are shown in the lower frequency range. The left one at 164.0 kHz, of known effective mass m_{eff} = 2.3 μg, is used to calibrate the spectra. The higher frequency range shows the hBN mode used for dynamical backaction experiments. Solid lines are theoretical fits using eq 1 with an additional constant noise floor.

frequency Ω_0, the mechanical line width Γ_0, the effective mass m_{eff} and an additional constant noise floor. The fit yields, assuming the sample is thermalized with the environment, $\Omega_0/2\pi$ = 1592.671(4) kHz, $\Gamma_0/2\pi$ = 525(10) Hz, quality factor Q = 3000(50), and m_{eff} = 1.2(1) ng for the hBN mode. The inferred zero-point fluctuations are $x_{zpf} = \sqrt{\hbar/(2m_{eff}\Omega_0)}$ = 2.1(1) fm which lead to a single-photon coupling strength of $g_0/2\pi = Gx_{zpf}/2\pi$ = 330 MHz/nm × 2.1 fm = 693 Hz. Since the effective mass was measured with the lock red detuned, the calculated value of g_0 is a lower limit to the real value. Finally, from the noise floor level we obtain a sensitivity of 15 fm/$\sqrt{Hz}$.

The mechanical resonator will experience an optomechanical force when the frequency of the probe laser ω_p is swept across the cavity resonance, with $\Delta_p = \omega_p - \omega_{cav}$ the probe detuning. This leads to the optical spring effect, a shift of the mechanical frequency $\Omega_m^2 = \Omega_0^2 + \delta(\Omega^2)$ that, when neglecting the dissipative coupling, is given by[48]

$$\delta(\Omega^2) = 2\Omega_0 g^2 \left(\frac{\Omega_0 + \Delta_p}{(\Omega_0 + \Delta_p)^2 + (\kappa/2)^2} - \frac{\Omega_0 - \Delta_p}{(\Omega_0 - \Delta_p)^2 + (\kappa/2)^2} \right) \quad (2)$$

where $g = \sqrt{n_p}g_0$ is the dispersive optomechanical coupling strength, n_p is the circulating probe photon number inside the cavity, and $g_0 = Gx_{zpf}$ the single-photon coupling strength. The mechanical line width experiences a shift as well, $\Gamma_m = \Gamma_0 + \Gamma_{opt}$, with Γ_{opt} the optomechanical damping. Considering negligible dissipative coupling, the latter reads[48]

$$\Gamma_{opt} = 2g^2\kappa \left(\frac{1}{(\Omega_0 + \Delta_p)^2 + (\kappa/2)^2} - \frac{1}{(\Omega_0 - \Delta_p)^2 + (\kappa/2)^2} \right) \quad (3)$$

In Figure 5 we demonstrate dynamical backaction by measuring the optical spring effect (Figure 5b) and optomechanical damping (Figure 5c) of the hBN mechanical mode in Figure 4. We scan the probe frequency across the cavity resonance using a constant probe power of P_p = 11 μW. For each probe detuning, we extract the circulating probe
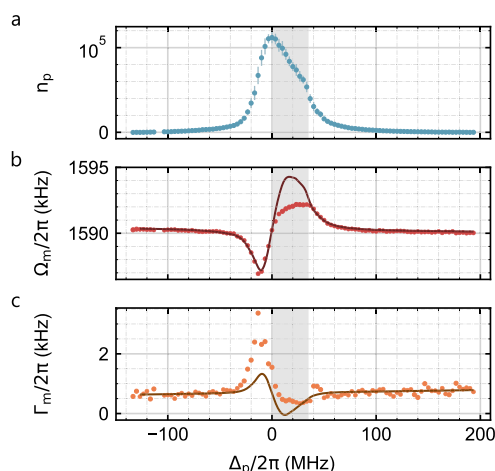
Figure 5. Radiation pressure backaction. (a) Experimental probe photon number n_p vs probe detuning Δ_p. (b) Optical spring effect (red dots) and theoretical regression (solid line). The gray region corresponds to the regime where the photon number shows a nonlinear response and its data are excluded in the fit. (c) Mechanical damping (orange dots) and theory calculation (solid line) with the parameters from the fit in (b). The error bars for Ω_m and Γ_m, generated from the fits to eq 1, are omitted because they are not appreciable in the figure.

photon number n_p inside the cavity from its transmission and measure the thermomechanical spectrum. We obtain the effective mechanical resonance frequency Ω_m and effective line width Γ_m by fitting eq 1 to the spectra. The circulating probe photon number (Figure 5a) appears to be nonlinear and is asymmetric with respect to probe detuning. Starting from positive detunings, the photon number increases in a Lorentzian fashion until $\Delta_p/2\pi$ = 35 MHz. Then, it increases almost linearly until reaching its maximum at $\Delta_p/2\pi$ = 0. After that, it drops with decreasing detuning, according to a Lorentzian trend. This behavior indicates the presence of a nonlinearity in the system that we will discuss in the next paragraphs.

The backaction of the probe leads to a softening (stiffening) of the mechanical frequency for negative (positive) detunings (Figure 5b, red dots), with a maximum frequency shift of $|\delta\Omega/2\pi|$ = 3 kHz for negative detunings. In addition, the natural frequency has a slight negative slope stemming from drifts in the lock that originate from changes of the sample position due to slow temperature drifts in the laboratory. The solid line is a fit to the optical spring using eq 2 together with a linear background. For the fit, we exclude the data points where the photon number shows a nonlinear response ($0 < \Delta_p/2\pi < 35$ MHz, gray shaded area in Figure 5b and Figure 5c). We also assume negligible dissipative coupling and feed the equation with the experimentally measured probe photon number n_p. The only free parameters for the fit are g_0 and the cavity line width κ. The best fit yields $g_0/2\pi$ = 1200(20) Hz and $\kappa/2\pi$ = 54(1) MHz. The data show an asymmetry around the probe detuning that is not predicted by the linear cavity optomechanics theory (eqs 2 and 3). We discard the possibility of an asymmetry induced by the dissipative coupling because of the small value of the single-photon dissipative coupling strength, $g_{0,\kappa}/2\pi = G_\kappa x_{zpf}/2\pi$ = 0.4 Hz. The asymmetry in the optical spring could be attributed to nonlinearities in the system given the large photon number reached in the experiments ($n_p > 10^5$). Indeed, a cavity optomechanical

system incorporating a negative Kerr nonlinearity can reproduce the asymmetries we observe.[56] Additional experiments should be conducted in the future to clarify the origin of the nonlinearity in the system. This could be due to, for example, the radiation pressure force itself[57] or to thermal effects given the absorption of the mirrors' coating.[42]

Figure 5c shows the effective line width Γ_m (orange dots) as a function of the probe detuning. The solid line is the result of eq 3 using the parameters obtained from the fit of the optical spring. We observe a larger broadening (optomechanical cooling) than what is predicted by the theory for negative detunings, whereas the narrowing (optomechanical heating) found for positive detunings is less pronounced compared to the theoretical model. This behavior also matches the one of a cavity optomechanical system with a negative Kerr nonlinearity,[56] which supports the hypothesis of a nonlinearity present in the system. In addition, the measured line widths are broadened due to unavoidable mechanical fluctuations of the positioning system and the fiber mirrors. The fluctuations translate into cavity length noise, which directly affects the detuning and therefore turns into mechanical frequency noise.[41,43] Because each experimental mechanical spectrum is the average of the mechanical response during the acquisition time of the spectrum analyzer, the experimental resonance frequency matches on average the theoretical value, besides the asymmetry already discussed. The mechanical line width (Figure 5c), however, is broadened especially for detunings at which Ω_m depends strongly on the detuning. The positioning system's mechanical fluctuations are also the limiting factor of this experiment and the reason we are unable to successfully lock the cavity at sample positions with a larger coupling G.

To conclude, we have demonstrated radiation pressure backaction on an hBN resonator at telecom wavelengths. The mechanical performance of our sample was limited by the hybridization to the modes of the low stress SiN membrane resonator and the mechanical imperfections originating from the dry transfer process. The former can be improved by using high stress Si_3N_4 as a support for the hBN drums, pushing the Si_3N_4 resonances to higher frequencies and allowing resolution of the distinct mode shapes, the latter by using more gentle transfer mechanisms like a wet transfer.[50] The setup presented in this work is very versatile: a careful design of the mirror coatings would enable the incorporation of several wavelengths, enabling photoluminescence experiments on-site. This will open the door to new ways of studying the strain dependence of hBN defects with an additional control of the mechanical properties through light and a new step forward toward the realization of spin-optomechanics with this van der Waals material.

ASSOCIATED CONTENT

Ⓢ Supporting Information

The Supporting Information is available free of charge at https://pubs.acs.org/doi/10.1021/acs.nanolett.3c00544.

Evidence of sample bulging, optical losses introduced by the circular frame, mechanical modes characterization, influence of the SiN membrane on the optomechanical couplings, and characterization of the dispersive optomechanical coupling of additional hBN devices (PDF)

AUTHOR INFORMATION

Corresponding Author

Eva M. Weig — *Department of Electrical Engineering, School of Computation, Information and Technology, Technical University of Munich, 85748 Garching, Germany; Munich Center for Quantum Science and Technology (MCQST), 80799 Munich, Germany; TUM Center for Quantum Engineering (ZQE), 85748 Garching, Germany;* Email: eva.weig@tum.de

Authors

Irene Sánchez Arribas — *Department of Electrical Engineering, School of Computation, Information and Technology, Technical University of Munich, 85748 Garching, Germany;* ⓞ orcid.org/0000-0003-1903-1678

Takashi Taniguchi — *International Center for Materials Nanoarchitectonics, National Institute for Materials Science, Tsukuba, Ibaraki 305-0044, Japan;* ⓞ orcid.org/0000-0002-1467-3105

Kenji Watanabe — *Research Center for Functional Materials, National Institute for Materials Science, Tsukuba, Ibaraki 305-0044, Japan;* ⓞ orcid.org/0000-0003-3701-8119

Complete contact information is available at:
https://pubs.acs.org/10.1021/acs.nanolett.3c00544

Author Contributions

I.S.A. fabricated the samples, constructed the setup, and carried out all the experiments. I.S.A. and E.M.W. analyzed and interpreted the data. T.T. and K.W. grew the hBN crystals. I.S.A. and E.M.W. contributed to writing the manuscript.

Notes

The authors declare no competing financial interest.

REFERENCES

(1) Aspelmeyer, M.; Kippenberg, T. J.; Marquardt, F. Cavity Optomechanics. *Rev. Mod. Phys.* **2014**, *86*, 1391−1452.

(2) Favero, I.; Karrai, K. Cavity Cooling of a Nanomechanical Resonator by Light Scattering. *New J. Phys.* **2008**, *10*, 095006.

(3) Stapfner, S.; Ost, L.; Hunger, D.; Reichel, J.; Favero, I.; Weig, E. M. Cavity-Enhanced Optical Detection of Carbon Nanotube Brownian Motion. *Appl. Phys. Lett.* **2013**, *102*, 151910.

(4) Barnard, A. W.; Zhang, M.; Wiederhecker, G. S.; Lipson, M.; McEuen, P. L. Real-Time Vibrations of a Carbon Nanotube. *Nature* **2019**, *566*, 89−93.

(5) Blien, S.; Steger, P.; Hüttner, N.; Graaf, R.; Hüttel, A. K. Quantum Capacitance Mediated Carbon Nanotube Optomechanics. *Nat. Commun.* **2020**, *11*, 1636.

(6) Fogliano, F.; Besga, B.; Reigue, A.; Heringlake, P.; Mercier de Lépinay, L.; Vaneph, C.; Reichel, J.; Pigeau, B.; Arcizet, O. Mapping the Cavity Optomechanical Interaction with Subwavelength-Sized Ultrasensitive Nanomechanical Force Sensors. *Phys. Rev. X* **2021**, *11*, 021009.

(7) Song, X.; Oksanen, M.; Li, J.; Hakonen, P. J.; Sillanpää, M. A. Graphene Optomechanics Realized at Microwave Frequencies. *Phys. Rev. Lett.* **2014**, *113*, 027404.

(8) Singh, V.; Bosman, S. J.; Schneider, B. H.; Blanter, Y. M.; Castellanos-Gomez, A.; Steele, G. A. Optomechanical Coupling between a Multilayer Graphene Mechanical Resonator and a Superconducting Microwave Cavity. *Nat. Nanotechnol.* **2014**, *9*, 820−824.

(9) Weber, P.; Güttinger, J.; Noury, A.; Vergara-Cruz, J.; Bachtold, A. Force Sensitivity of Multilayer Graphene Optomechanical Devices. *Nat. Commun.* **2016**, *7*, 12496.

(10) Williamson, I. A. D.; Mousavi, S. H.; Wang, Z. Large Cavity-Optomechanical Coupling with Graphene at Infrared and Terahertz Frequencies. *ACS Photonics* **2016**, *3*, 2353−2361.

(11) Brennecke, F.; Ritter, S.; Donner, T.; Esslinger, T. Cavity Optomechanics with a Bose−Einstein Condensate. *Science* **2008**, *322*, 235−238.

(12) Leijssen, R.; La Gala, G. R.; Freisem, L.; Muhonen, J. T.; Verhagen, E. Nonlinear Cavity Optomechanics with Nanomechanical Thermal Fluctuations. *Nat. Commun.* **2017**, *8*, ncomms16024.

(13) Peterson, G. A.; Kotler, S.; Lecocq, F.; Cicak, K.; Jin, X. Y.; Simmonds, R. W.; Aumentado, J.; Teufel, J. D. Ultrastrong Parametric Coupling between a Superconducting Cavity and a Mechanical Resonator. *Phys. Rev. Lett.* **2019**, *123*, 247701.

(14) Zheng, X.-Q.; Lee, J.; Feng, P. X.-L. Hexagonal Boron Nitride Nanomechanical Resonators with Spatially Visualized Motion. *Microsyst. Nanoeng.* **2017**, *3*, 17038.

(15) Falin, A.; Cai, Q.; Santos, E. J. G.; Scullion, D.; Qian, D.; Zhang, R.; Yang, Z.; Huang, S.; Watanabe, K.; Taniguchi, T.; Barnett, M. R.; Chen, Y.; Ruoff, R. S.; Li, L. H. Mechanical Properties of Atomically Thin Boron Nitride and the Role of Interlayer Interactions. *Nat. Commun.* **2017**, *8*, 15815.

(16) Elbadawi, C.; Tran, T. T.; Kolíbal, M.; Šikola, T.; Scott, J.; Cai, Q.; Li, L. H.; Taniguchi, T.; Watanabe, K.; Toth, M.; Aharonovich, I.; Lobo, C. Electron Beam Directed Etching of Hexagonal Boron Nitride. *Nanoscale* **2016**, *8*, 16182−16186.

(17) Kim, S.; Fröch, J. E.; Christian, J.; Straw, M.; Bishop, J.; Totonjian, D.; Watanabe, K.; Taniguchi, T.; Toth, M.; Aharonovich, I. Photonic Crystal Cavities from Hexagonal Boron Nitride. *Nat. Commun.* **2018**, *9*, 2623.

(18) Cassabois, G.; Valvin, P.; Gil, B. Hexagonal Boron Nitride Is an Indirect Bandgap Semiconductor. *Nature Photon* **2016**, *10*, 262−266.

(19) Barton, R. A.; Storch, I. R.; Adiga, V. P.; Sakakibara, R.; Cipriany, B. R.; Ilic, B.; Wang, S. P.; Ong, P.; McEuen, P. L.; Parpia, J. M.; Craighead, H. G. Photothermal Self-Oscillation and Laser Cooling of Graphene Optomechanical Systems. *Nano Lett.* **2012**, *12*, 4681−4686.

(20) Meyer, H. M.; Breyer, M.; Köhl, M. Monolayer Graphene as Dissipative Membrane in an Optical Resonator. *Appl. Phys. B* **2016**, *122*, 290.

(21) Morell, N.; Tepsic, S.; Reserbat-Plantey, A.; Cepellotti, A.; Manca, M.; Epstein, I.; Isacsson, A.; Marie, X.; Mauri, F.; Bachtold, A. Optomechanical Measurement of Thermal Transport in Two-Dimensional MoSe2 Lattices. *Nano Lett.* **2019**, *19*, 3143−3150.

(22) Kubanek, A. Coherent Quantum Emitters in Hexagonal Boron Nitride. *Advanced Quantum Technologies* **2022**, *5*, 2200009.

(23) Aharonovich, I.; Tetienne, J.-P.; Toth, M. Quantum Emitters in Hexagonal Boron Nitride. *Nano Lett.* **2022**, *22*, 9227−9235.

(24) Grosso, G.; Moon, H.; Lienhard, B.; Ali, S.; Efetov, D. K.; Furchi, M. M.; Jarillo-Herrero, P.; Ford, M. J.; Aharonovich, I.; Englund, D. Tunable and High-Purity Room Temperature Single-Photon Emission from Atomic Defects in Hexagonal Boron Nitride. *Nat. Commun.* **2017**, *8*, 705.

(25) Li, S.; Chou, J.-P.; Hu, A.; Plenio, M. B.; Udvarhelyi, P.; Thiering, G.; Abdi, M.; Gali, A. Giant Shift upon Strain on the Fluorescence Spectrum of VNNB Color Centers in h-BN. *npj Quantum Inf.* **2020**, *6*, 85.

(26) Noh, G.; Choi, D.; Kim, J.-H.; Im, D.-G.; Kim, Y.-H.; Seo, H.; Lee, J. Stark Tuning of Single-Photon Emitters in Hexagonal Boron Nitride. *Nano Lett.* **2018**, *18*, 4710−4715.

(27) Nikolay, N.; Mendelson, N.; Sadzak, N.; Böhm, F.; Tran, T. T.; Sontheimer, B.; Aharonovich, I.; Benson, O. Very Large and Reversible Stark-Shift Tuning of Single Emitters in Layered Hexagonal Boron Nitride. *Phys. Rev. Appl.* **2019**, *11*, 041001.

(28) Kianinia, M.; Regan, B.; Tawfik, S. A.; Tran, T. T.; Ford, M. J.; Aharonovich, I.; Toth, M. Robust Solid-State Quantum System Operating at 800 K. *ACS Photonics* **2017**, *4*, 768−773.

(29) Gottscholl, A.; Kianinia, M.; Soltamov, V.; Orlinskii, S.; Mamin, G.; Bradac, C.; Kasper, C.; Krambrock, K.; Sperlich, A.; Toth, M.; Aharonovich, I.; Dyakonov, V. Initialization and Read-out of Intrinsic Spin Defects in a van Der Waals Crystal at Room Temperature. *Nat. Mater.* **2020**, *19*, 540−545.

(30) Gao, X.; Pandey, S.; Kianinia, M.; Ahn, J.; Ju, P.; Aharonovich, I.; Shivaram, N.; Li, T. Femtosecond Laser Writing of Spin Defects in Hexagonal Boron Nitride. *ACS Photonics* **2021**, *8*, 994−1000.

(31) Stern, H. L.; Gu, Q.; Jarman, J.; Eizagirre Barker, S.; Mendelson, N.; Chugh, D.; Schott, S.; Tan, H. H.; Sirringhaus, H.; Aharonovich, I.; Atatüre, M. Room-Temperature Optically Detected Magnetic Resonance of Single Defects in Hexagonal Boron Nitride. *Nat. Commun.* **2022**, *13*, 618.

(32) Gottscholl, A.; Diez, M.; Soltamov, V.; Kasper, C.; Sperlich, A.; Kianinia, M.; Bradac, C.; Aharonovich, I.; Dyakonov, V. Room Temperature Coherent Control of Spin Defects in Hexagonal Boron Nitride. *Sci. Adv.* **2021**, *7*, No. eabf3630.

(33) Gao, X.; Jiang, B.; Llacsahuanga Allcca, A. E.; Shen, K.; Sadi, M. A.; Solanki, A. B.; Ju, P.; Xu, Z.; Upadhyaya, P.; Chen, Y. P.; Bhave, S. A.; Li, T. High-Contrast Plasmonic-Enhanced Shallow Spin Defects in Hexagonal Boron Nitride for Quantum Sensing. *Nano Lett.* **2021**, *21*, 7708−7714.

(34) Ramsay, A. J.; Hekmati, R.; Patrickson, C. J.; Baber, S.; Arvidsson-Shukur, D. R. M.; Bennett, A. J.; Luxmoore, I. J. Coherence Protection of Spin Qubits in Hexagonal Boron Nitride. *Nat. Commun.* **2023**, *14*, 461.

(35) Gottscholl, A.; Diez, M.; Soltamov, V.; Kasper, C.; Krauße, D.; Sperlich, A.; Kianinia, M.; Bradac, C.; Aharonovich, I.; Dyakonov, V. Spin Defects in hBN as Promising Temperature, Pressure and Magnetic Field Quantum Sensors. *Nat. Commun.* **2021**, *12*, 4480.

(36) Lyu, X.; Tan, Q.; Wu, L.; Zhang, C.; Zhang, Z.; Mu, Z.; Zúñiga-Pérez, J.; Cai, H.; Gao, W. Strain Quantum Sensing with Spin Defects in Hexagonal Boron Nitride. *Nano Lett.* **2022**, *22*, 6553−6559.

(37) Abdi, M.; Hwang, M.-J.; Aghtar, M.; Plenio, M. B. Spin-Mechanical Scheme with Color Centers in Hexagonal Boron Nitride Membranes. *Phys. Rev. Lett.* **2017**, *119*, 233602.

(38) Wang, H.; Lekavicius, I. Coupling Spins to Nanomechanical Resonators: Toward Quantum Spin-Mechanics. *Appl. Phys. Lett.* **2020**, *117*, 230501.

(39) Shandilya, P. K.; Fröch, J. E.; Mitchell, M.; Lake, D. P.; Kim, S.; Toth, M.; Behera, B.; Healey, C.; Aharonovich, I.; Barclay, P. E. Hexagonal Boron Nitride Cavity Optomechanics. *Nano Lett.* **2019**, *19*, 1343−1350.

(40) Liu, Y.; Wang, Y.; Zheng, X.-Q.; Lin, Q.; Feng, P. X.-L. Nanomechanical and Optomechanical Coupling in Silicon Carbide/Hexagonal Boron Nitride Hybrid Resonator. *2021 21st International Conference on Solid-State Sensors, Actuators and Microsystems (Transducers)*; IEEE, 2021; pp 541−544.

(41) Rochau, F.; Sánchez Arribas, I.; Brieussel, A.; Stapfner, S.; Hunger, D.; Weig, E. M. Dynamical Backaction in an Ultrahigh-Finesse Fiber-Based Microcavity. *Phys. Rev. Appl.* **2021**, *16*, 014013.

(42) Hunger, D.; Steinmetz, T.; Colombe, Y.; Deutsch, C.; Hänsch, T. W.; Reichel, J. A Fiber Fabry−Perot Cavity with High Finesse. *New J. Phys.* **2010**, *12*, 065038.

(43) Flowers-Jacobs, N. E.; Hoch, S. W.; Sankey, J. C.; Kashkanova, A.; Jayich, A. M.; Deutsch, C.; Reichel, J.; Harris, J. G. E. Fiber-Cavity-Based Optomechanical Device. *Appl. Phys. Lett.* **2012**, *101*, 221109.

(44) Pfeifer, H.; Ratschbacher, L.; Gallego, J.; Saavedra, C.; Faßbender, A.; von Haaren, A.; Alt, W.; Hofferberth, S.; Köhl, M.; Linden, S.; Meschede, D. Achievements and Perspectives of Optical Fiber Fabry–Perot Cavities. *Appl. Phys. B* **2022**, *128*, 29.

(45) Thompson, J. D.; Zwickl, B. M.; Jayich, A. M.; Marquardt, F.; Girvin, S. M.; Harris, J. G. E. Strong Dispersive Coupling of a High-Finesse Cavity to a Micromechanical Membrane. *Nature* **2008**, *452*, 72–75.

(46) Jayich, A. M.; Sankey, J. C.; Zwickl, B. M.; Yang, C.; Thompson, J. D.; Girvin, S. M.; Clerk, A. A.; Marquardt, F.; Harris, J. G. E. Dispersive Optomechanics: A Membrane inside a Cavity. *New J. Phys.* **2008**, *10*, 095008.

(47) Sankey, J. C.; Yang, C.; Zwickl, B. M.; Jayich, A. M.; Harris, J. G. E. Strong and Tunable Nonlinear Optomechanical Coupling in a Low-Loss System. *Nature Phys.* **2010**, *6*, 707–712.

(48) Biancofiore, C.; Karuza, M.; Galassi, M.; Natali, R.; Tombesi, P.; Di Giuseppe, G.; Vitali, D. Quantum Dynamics of an Optical Cavity Coupled to a Thin Semitransparent Membrane: Effect of Membrane Absorption. *Phys. Rev. A* **2011**, *84*, 033814.

(49) Castellanos-Gomez, A.; Buscema, M.; Molenaar, R.; Singh, V.; Janssen, L.; van der Zant, H. S. J.; Steele, G. A. Deterministic Transfer of Two-Dimensional Materials by All-Dry Viscoelastic Stamping. *2D Mater.* **2014**, *1*, 011002.

(50) Jaeger, D.; Fogliano, F.; Ruelle, T.; Lafranca, A.; Braakman, F.; Poggio, M. Mechanical Mode Imaging of a High-Q Hybrid hBN/Si3N4 Resonator. *Nano Lett.* **2023**, *23*, 2016–2022.

(51) Karuza, M.; Galassi, M.; Biancofiore, C.; Molinelli, C.; Natali, R.; Tombesi, P.; Di Giuseppe, G.; Vitali, D. Tunable Linear and Quadratic Optomechanical Coupling for a Tilted Membrane within an Optical Cavity: Theory and Experiment. *J. Opt.* **2013**, *15*, 025704.

(52) Katsidis, C. C.; Siapkas, D. I. General Transfer-Matrix Method for Optical Multilayer Systems with Coherent, Partially Coherent, and Incoherent Interference. *Appl. Opt., AO* **2002**, *41*, 3978–3987.

(53) Rah, Y.; Jin, Y.; Kim, S.; Yu, K. Optical Analysis of the Refractive Index and Birefringence of Hexagonal Boron Nitride from the Visible to Near-Infrared. *Opt. Lett., OL* **2019**, *44*, 3797–3800.

(54) Lee, S.-Y.; Jeong, T.-Y.; Jung, S.; Yee, K.-J. Refractive Index Dispersion of Hexagonal Boron Nitride in the Visible and Near-Infrared. *physica status solidi (b)* **2019**, *256*, 1800417.

(55) Hauer, B. D.; Doolin, C.; Beach, K. S. D.; Davis, J. P. A General Procedure for Thermomechanical Calibration of Nano/Micro-Mechanical Resonators. *Annals of Physics* **2013**, *339*, 181–207.

(56) Zoepfl, D.; Juan, M. L.; Diaz-Naufal, N.; Schneider, C. M. F.; Deeg, L. F.; Sharafiev, A.; Metelmann, A.; Kirchmair, G. Kerr Enhanced Backaction Cooling in Magnetomechanics. *Phys. Rev. Lett.* **2023**, *130*, 033601.

(57) Dorsel, A.; McCullen, J. D.; Meystre, P.; Vignes, E.; Walther, H. Optical Bistability and Mirror Confinement Induced by Radiation Pressure. *Phys. Rev. Lett.* **1983**, *51*, 1550–1553.